Microstructural and Mechanical Properties of As Built, Solution Treated and Aged 18 Ni (300 grade) Maraging Steel Produced by Selective Laser Melting

R. Casati, J. Lemke, M. Vedani

Mechanical and microstructural properties of 18-Ni (300 grade) maraging steel processed by selective laser melting were investigated to evaluate the effect of the peculiar processing conditions and of the subsequent heat treatment. No need of solution treatment prior to aging revealed necessary owing to the rapid cooling rate experienced by the material during selective laser melting. Isothermal aging temperature and time played a main role in promoting austenite reversion. Aging also induced a dramatic increase in strength with respect to the as-built condition and a decrease in fracture elongation. It is proposed that tensile strength and ductility are mainly governed by the effects brought by the strengthening precipitates, whereas the concurrent reversion of martensite into austenite is likely to play a minor role. Analysis of defects induced by selective laser melting process and on fracture behavior of the tensile specimens allowed to improve the understanding of materials performance and to draw guideline for process improvement.

KEYWORDS: ADDITIVE MANUFACTURING - SELECTIVE LASER MELTING - MARAGING STEEL - AGING

INTRODUCTION

Maraging steels are low-carbon ultra-high strength iron alloys with good toughness that derive their mechanical properties from the aging of a relatively soft Ni-rich martensite. It is reported that in the 18-Ni 300 alloy and in similar grades, Ni-based precipitates (mainly Ni_3Ti, Ni_3Mo) are formed in a first stage of aging, whereas Fe-based precipitates (Fe_2Mo and Fe_7Mo_6) replace in a second stage the previously formed species. Furthermore, aging treatment leads to austenite reversion that is stimulated by the release of Ni into the matrix due to the decomposition of the Ni_3Ti and Ni_3Mo precipitates. Over-aging may promote softening and increases crack blunting effects due to the formation of high austenite fraction, however this beneficial influence may be counterbalanced by matrix embrittlement due to precipitate growing and coarsening [1-6].

Recently, maraging steels have been successfully processed by selective laser melting (SLM), an additive manufacturing (AM) technique based on the local fusion of a powder bed by a laser beam [7-10]. Fully dense parts featuring mechanical properties that are commonly better than those produced by casting are manufactured by SLM thanks to the refined microstructure generated during cooling [7-11]. In fact, the high local energy and the fast scans of the laser are responsible for large thermal gradients and fast cooling rates [12,13]. The localized thermal cycles inducing rapid melting and cooling are also the cause of complex fluid flows within the melt pool that may lead to microstructural defects. Several processing parameters, including layer thickness, scanning strategy, hatch distance, spot size, focus, and power of the laser must be adjusted so as to minimize the generation of small solidification faults, such as pores, incompletely melted particles and material spattering from melt pools, which in turn are responsible for the formation of un-melted zones and fusion defects [12-14]. Microstructural heterogeneities can strongly deteriorate mechanical behavior of AM components, especially when materials with low damage-tolerant ability are employed and they can constitute a limitation for the manufacturing of reliable structural parts, especially if they are subjected to cyclic loading in service.

R. Casati, J. Lemke, M. Vedani
Department of Mechanical Engineering,
Politecnico di Milano,
Via La Masa 34, Milano, Italy

The aim of the present study consisted in studying the microstructure, hardness and tensile properties of 18-Ni (300 grade) maraging steel bars prepared by SLM as a function of tailored aging treatments. Emphasis is also put on fracture behavior of the materials and on process-induced microstructural defects in order to improve the understanding about performance of SLM materials as affected by processing conditions.

Materials and Methods

Gas-atomized 18-Ni 300 maraging steel powder supplied by Sandvik Osprey LTD was used for the experiments. A representative micrograph of the powder is shown in Figure 1. The alloy chemical composition is given in Table 1.

Tab. 1 - Chemical composition in weight percent (wt.%) of the 18-Ni 300 maraging steel powder.

Ni	Mo	Co	Ti	Al	Si	Fe
17.6	5.3	9.6	0.7	0.09	0.2	Bal.

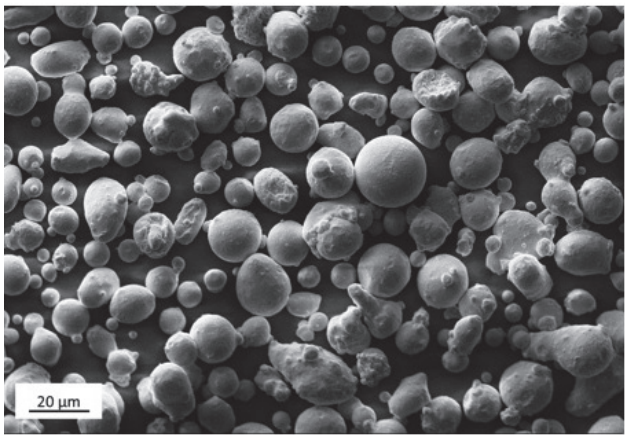

Fig. 1 - View of the gas-atomized 18-Ni 300 alloy powder used for the experiments.

A Renishaw AM250 SLM system, which has installed a single mode fiber laser with a power of 200 W and an estimated beam diameter at focal point of 75 µm, was used to produce a set of samples consisting of horizontal and vertical bars (10 mm x 10 mm x 75 mm). Block-type support were built to join parts together with the carbon steel build plate. In Figure 2, a close-up view of the supports and overlying bars is shown. Laser melting was performed by discrete and partially overlapped spots exposed to the radiation for a fixed time (t = 80 µs). After completing a line, the laser scans a partially overlapped adjacent line. Point distance and hatch distance were set at 65 µm and 80 µm, respectively, whereas thickness of each powder layer was set to 40 µm. Samples were produced under Ar atmosphere and by rotating the laser scanning direction by 67° after each layer in order to reduce residual stresses and crystallographic textures. The built parts were removed from build plate and machined in order to produce cylindrical dog-bone specimens having a gauge length of 20 mm and a diameter of 4 mm.

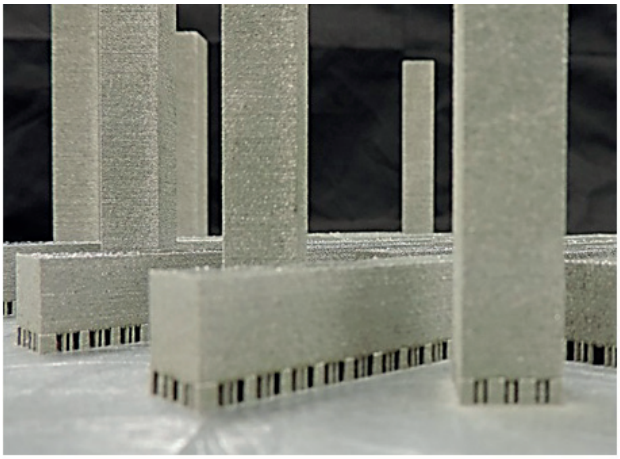

Fig. 2 - Close-up picture of the supports used for the build.

Microstructural analysis was carried out by scanning electron microscope (SEM) equipped with energy dispersive X-ray analysis (EDX) and electron backscattered diffraction (EBSD) detectors and by optical microscope after etching with Picral or modified Fry's solution.

Tensile tests were performed at room temperature with a crosshead speed of 0.5 mm/min using a MTS Alliance RT/100 universal testing machine equipped with extensometer. At least three specimens for each condition were tested.

Aging response of the samples was evaluated starting from the as-built condition or after a standard solution treatment, carried out at 815 °C for 30 min, followed by water quenching. Isothermal aging curves were then collected at 460, 490, 540, and 600 °C for times ranging from 10 min up to 14 days; hardness evolution was evaluated by performing Vickers indentations with 2 kg_F load.

Differential scanning calorimetry (DSC, Labsys Setaram) analyses were carried at 20, 30 and 40 °C/min in Ar atmosphere to assess precipitation sequence of strengthening phases. Kissinger method was used to calculate the activation energies of selected samples [15].

X-ray diffraction (XRD) patterns were collected using a X-Pert PRO PANalitical instrument equipped with a RTMS X'Celerator sensor. Cu Kα (k = 0.15418 nm) radiation was employed. Quantitative analysis of identified phases was implemented by Rietveld refinement method using Maud software [16].

RESULTS AND DISCUSSION

The process of powder consolidation by laser melting involves the generation of a multitude of small weld beads that can be readily recognized in low-magnification images taken from top of processed samples, as depicted in Figure 3. Partial overlapping of the laser tracks both along the build direction (normal to the plane of the figure) and laterally are here highlighted.

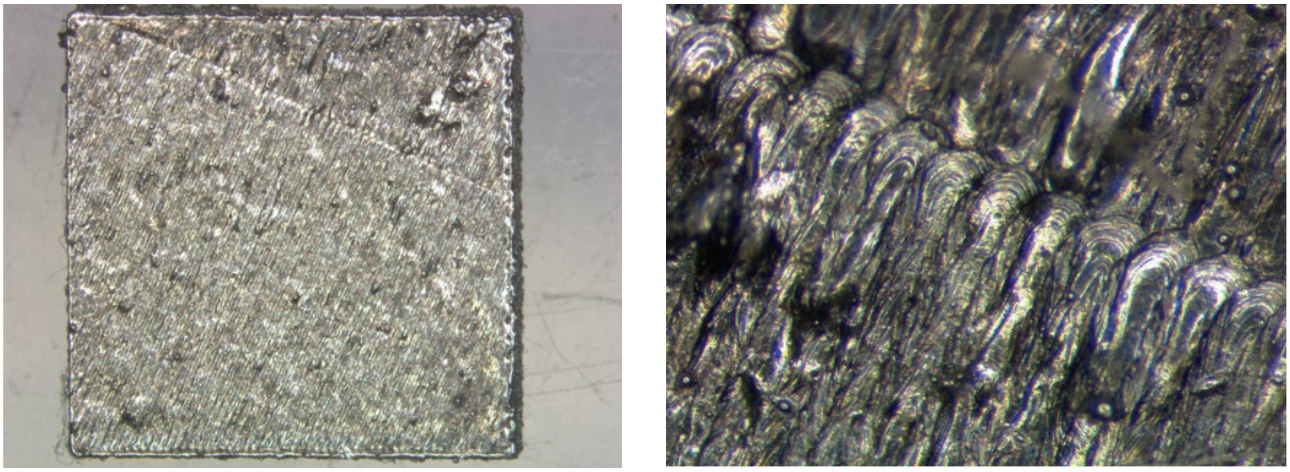

a. b.

Fig. 3 - Stereomicroscope images highlighting partial overlapping of the laser tracks

SEM analysis showing the top surface of samples (figure 4) revealed that a number of almost spherical particles are deposited, as a result of the rapid and intense melting process induced by the focused laser beam, also generating droplets of molten metals (commonly called splats) that are expelled from the pool, dragged by the inert gas flow and occasionally fall on the surface of the already consolidated metals, partially welding on it. The fairly large size of the particles suggests that these are not always the original powder particles but most of them are produced directly from a volume of the molten alloy. In Figure 5 a plot showing the normal distribution of the measured size of splats and of the original powder particles is reported to confirm this hypothesis.

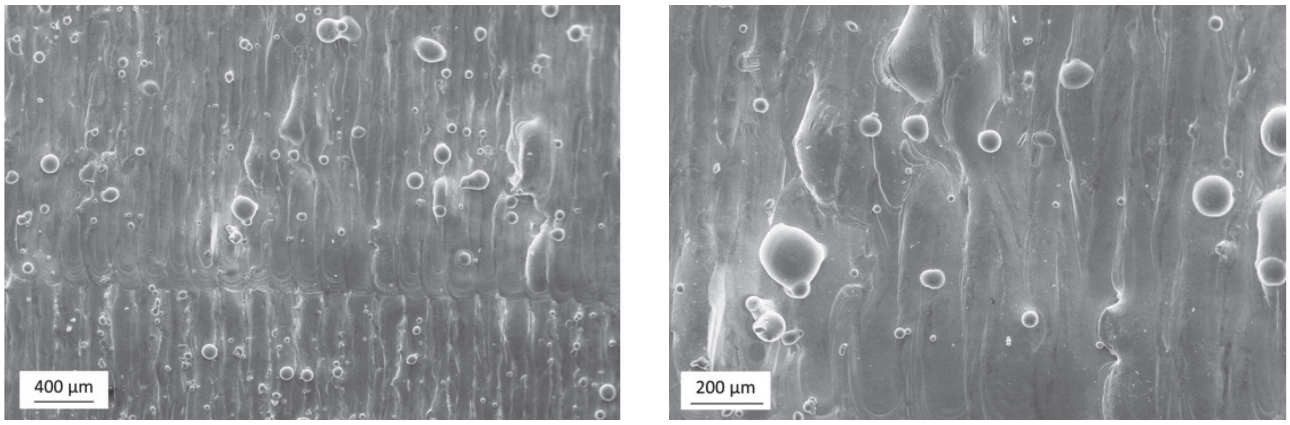

a. b.

Fig. 4 - SEM images showing splats deposited on the last layer at (a) low and (b) higher magnification.

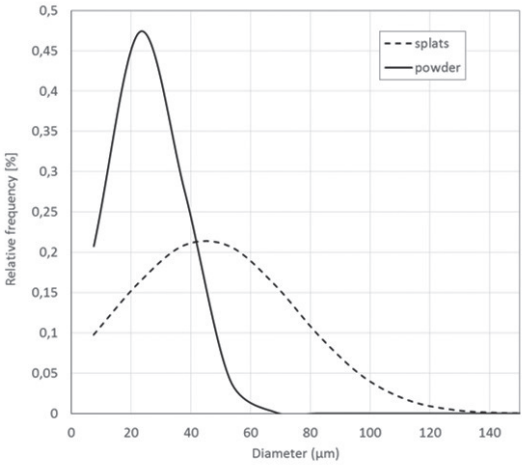

Fig. 5 - Normal distribution of the size of splats welded on the consolidated surface and original powder particles.

Figure 6 shows representative optical micrographs of the top and lateral sections of the as built parts after etching. At low magnification, the microstructure of the as build samples shows features similar to those observed from top external surfaces (see Figure 3 and Figure 4) consisting of multiple aligned weld beads. It is worth noting that the laser scanning direction rotates by 67° after each layer, leading to differently oriented melt pools. This reflects on different shape and size of cross-sectioned melt pools that can be observed from micrographs in Figure 6b. From the size (especially the depth) of the beads it is inferred that each single laser scan involves more than one single powder layer (the deposited layer has a nominal thickness of 40 mm) and re-melting of the consolidated material occurs, at least also for the second but last layer.

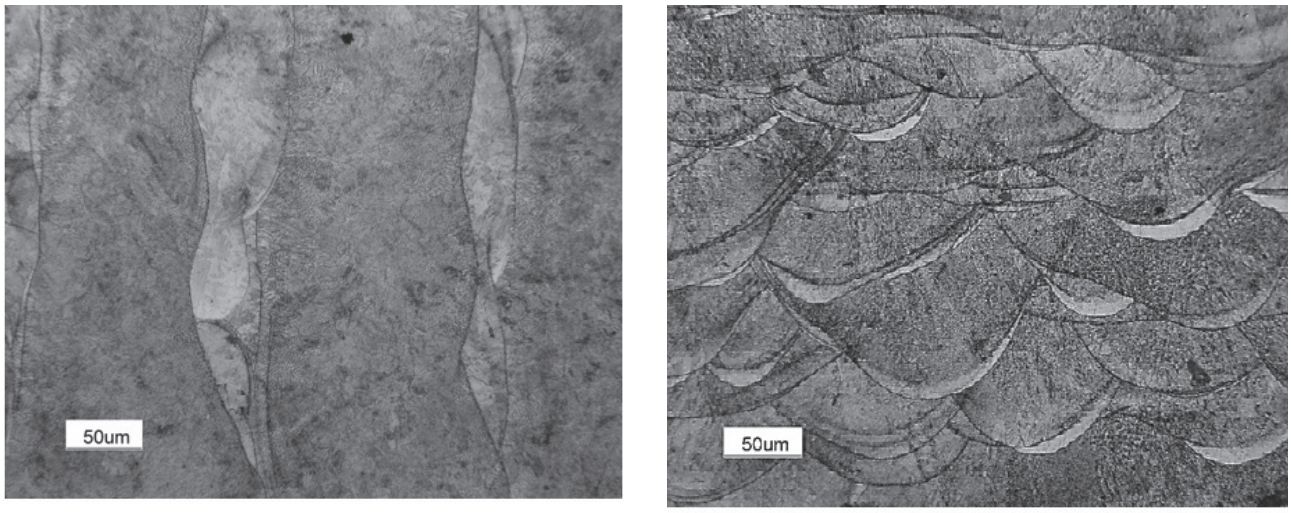

a. b.

Fig. 6 - Optical micrographs of the as built microstructure of the maraging steel: (a) Top view; and (b) Lateral view.

High magnification SEM micrograph shown in Figure 7 reveal a cellular solidification structure, typical of SLM processed parts [17-20], with cells smaller than 1 µm in diameter. Epitaxial growth of cellular dendrites from adjacent tracks can also be noticed. It is known that cooling rates of the melt pool in the order of 10^3–10^8 K·s^{-1} occur during SLM [21] and materials experience local melting and rapid solidification far from equilibrium conditions, which is driven by temperature gradients in the order of 10^6 K·m^{-1} [22]. According to ref. [23], the higher Ni-content segregated at cell boundaries owing to rapid process leads to the local formation of austenite. Accordingly, austenite can be readily recognized in micrographs of as built samples as the bright phase that decorates cell boundaries.

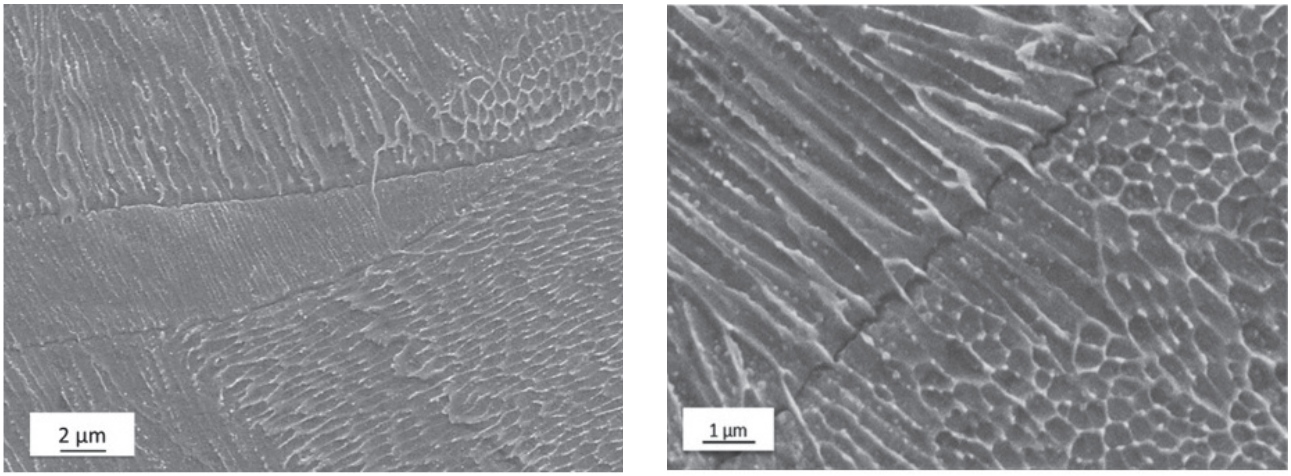

a. b.

Fig. 7 - SEM micrographs (a) at lower and (b) at higher magnification of the cellular solidification microstructure.

Solution treatment promote a radical changes in microstructure, as shown by the optical micrograph in Figure 8: the melt pool traces fully disappear and the cellular solidification structure is replaced by a lath martensite structure. A more detailed description of microstructural features for these samples is reported in ref. 24.

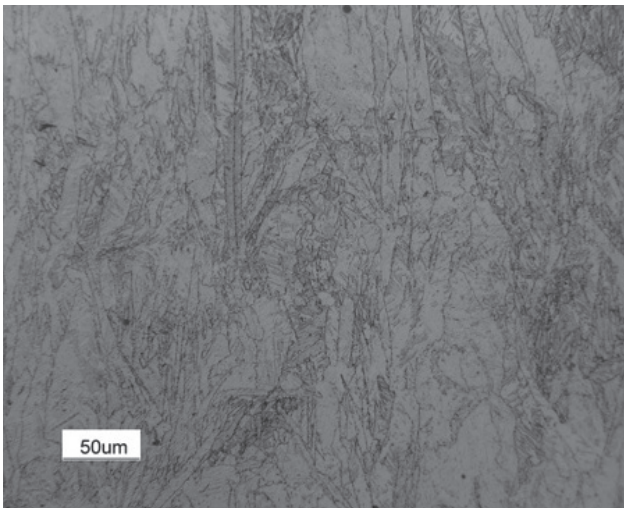

Fig. 8 - Optical micrograph of the solution treated sample.

The aging response of the SLMed 18-Ni 300 grade steel was studied by DSC analysis. In Figure 9, the results of DSC scans performed on the as build and solution annealed materials are shown. The two samples show similar calorimetric curves which are first marked by two exothermic peaks followed by two endothermic peaks. The first exothermic peak is believed to be produced by the formation of coherent precipitation zones, whereas the second is associated to the formation of the main strengthening precipitates, namely the Ni_3Ti and Ni_3Mo phases followed by the Fe_2Mo or Fe_7Mo_6 phases. The third and fourth endothermic peaks are instead caused by the austenite reversion and to the dissolution of precipitates [1–4, 24-27].

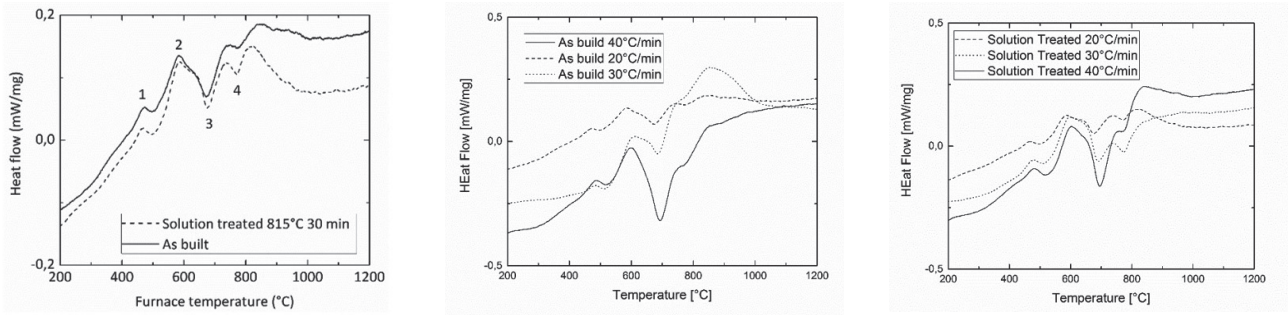

a. b. c.

Fig. 9 - Comparison of the DSC curves (a) of the as-built and solution-treated samples at heating rate of 20 °C/min; DSC curves of (b) the as-built and (c) the solution-treated samples at 20, 30 and 40 °C/min.

DSC data were also collected at heating rates of 20°C/min and 30°C/min in order to perform kinetic analysis by Kissinger method [15]. The assessed activation energies are summarized in Table 2. Since the first peak is related to a transformation driven by short-range diffusion, namely the formation of small coherent clusters of atoms, there are small differences in activation energies between the as build and the solution treated samples, which are about 205 kJ/mol. On the contrary, the processes related to long-range diffusion show larger differences: the activation energies referred to the strengthening precipitates formation for the as built and the solution treated samples are 174.5 and 274.4 kJ/mol, respectively; those related to the austenite reversion are 264.2 and 310.3 kJ/mol, respectively. The as built samples likely contain higher amount of crystal defects, such as cell boundaries and dislocations formed during fast cooling, than the solution treated sample. These defects act as preferential paths for atom migration, accelerating the diffusion-controlled precipitation reaction. Several authors found similar activation energy values for strengthening precipitates formation in maraging steels produced by conventional methods. Sha et al. [25] reported an activation energy of 205.1 kJ/mol in the case of wrought 250 grade maraging steel while Kapoor and Batra [26] found a value of 265 kJ/mol in a 350 grade maraging steel. Menapace et al. [27] obtained values of 150 kJ/mol and 269 kJ/mol corresponding to a 300 maraging steels sintered in two different conditions; the dissimilar energy values were also attributed to the differences in grain sizes and defect densities. For austenite reversion, activation energy values of 342 kJ/mol and of 423 kJ/mol were reported in literature [25,26], which are closer to those obtained for the solution treated sample.

Tab. 2 - Activation energies calculated from DSC curves by the Kissinger method.

Peak 1 E_a (kJ/mol)		Peak 2 E_a (kJ/mol)		Peak 3 E_a (kJ/mol)		Peak 4 E_a (kJ/mol)	
As built	Solution Treated	As built	Solution Treated	As built	Solution Treated	As built	Solution Treated
205.0	205.7	174.5	274.4	264.2	310.3	1406.8	1189.5

Isothermal aging was carried out at 460°C on the as build and solution treated coupons to evaluate possible differences in achievable strength. The hardness values as a function of the aging time is reported in Figure 10. The annealing performed at 815°C led to a drastic hardness drop, from 371 to 279 HV, probably due to stress relieving effect and slight microstructural coarsening. Moreover, it should be considered that in situ heat treatment might have been occurred during SLM that might have caused the formation of coherent precipitates or atom clustering in solute-rich zones, which might have been dissolved by solution treatment. However, this gap in hardness is readily bridged after only 30 min at 460 °C. Slightly higher peak hardness is reached after 8 hours by the as built sample (632 HV) than by the solution annealed alloy (613 HV).

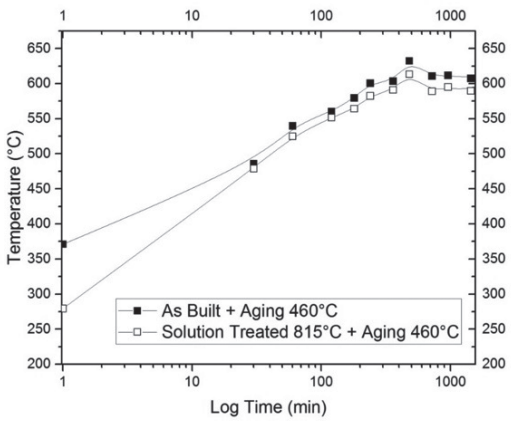

Fig. 10 - Hardness evolution of the as built and solution treated samples during isothermal holding at 460 °C.

From the present results it can be deduced that the solidification and cooling rates induced by SLM processing are fast enough to almost fully preserve the aging potential of the 18-Ni 300 maraging alloy, without any need to perform an additional post-SLM solution treatment to dissolve second phases.
Aging test were also performed at 490, 540 and 600 °C starting from as built samples. The evolution of hardness during aging at the above temperatures is shown in Figure 11. Peak hardness condition is reached after 4 h, 1 h and 10 min as temperature is increased from 490 to 540 and 600 °C. Long term exposure at 460 and 490 °C led to moderate loss in hardness, whereas over-aging effect was more severe in high-temperature annealed samples. Based on the above mentioned results, further tensile tests and XRD analysis were performed on as built samples, on peak aged samples treated at the different temperatures and on a further set of samples annealed for 8 h at 540 °C, which allows comparisons with the 600 °C peak-aged samples (similar hardness attained by different aging times) and the 460 °C peak-aged samples (same aging time but different attained hardness).

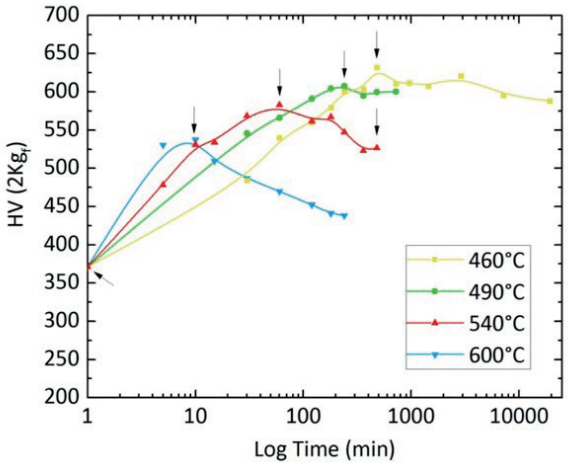

Fig. 11 - Hardness evolution of the as built samples during isothermal holding at 460, 490, 540 and 600 °C.

Aging induces an increase of austenite over martensite fraction, both aging temperature and time are effective in enhancing the amount of γ-phase [24]. The increase in austenite can also be readily observed in microstructure of aged samples. By way of example, the micrographs of samples aged at 460°C and 540°C for 8 h reported in Figure 12 clearly show an increase of the bright phase decorating the cell boundaries. A previous research work referred to welding of a wrought 18-Ni 250 maraging steel [28] reports that the as-welded microstructure might contain segregation of Mo and Ti at cell boundaries. Mo can enhance the austenite reversion transformation on aging due to early formation of Fe_2Mo, resulting in local enrichment in Ni of the matrix. A similar effect is expected to be active also in the rapidly solidified samples here investigated. Microstructure observations confirmed that austenite reversion on aging first occurred at cell boundaries and only on over-aging (8 h at 540°C), austenite forms at intracellular sites.

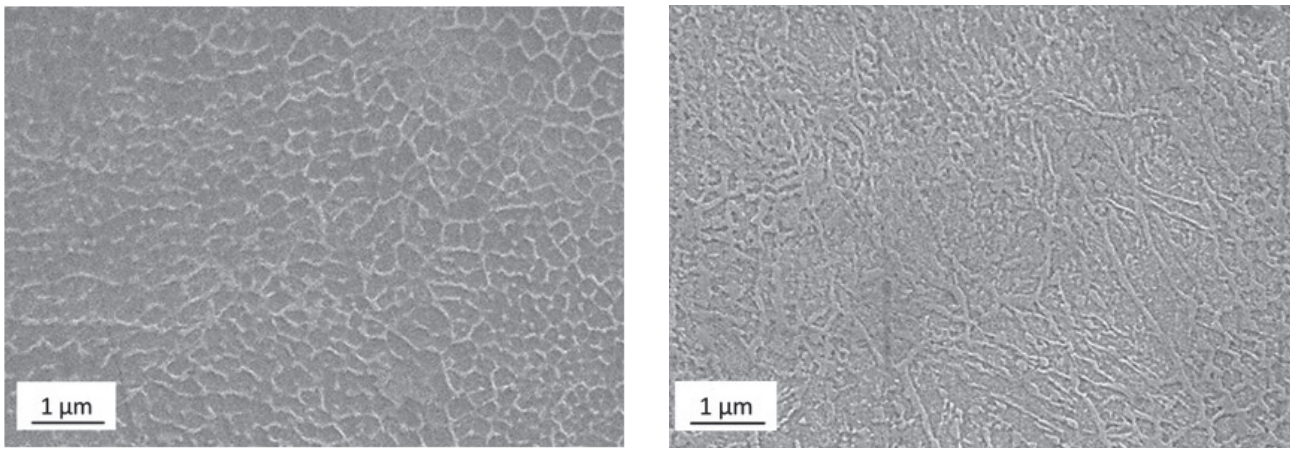

a. b.

Fig. 12 - Top view of SLMed 18-Ni 300 steel samples aged at (a) 460 °C 8 h and (a) 540 °C 8 h.

The histogram reported in Figure 13 summarize the results obtained from tensile tests. Vertically built specimens exhibit worse ductility and lower strength than those horizontally oriented. The different mechanical behavior is the result of the layer-by-layer fabrication process. It can be supposed that the production technique causes the preferential orientation of defects on planes normal to build direction since un-melted zones and fusion defects preferably occur at the interface among different layers. In vertical samples the loading direction is orthogonal to the un-melted interfaces, while in horizontal ones it is parallel to them. Therefore, defects more likely act as stress raisers and produce a more significant strength/ductility drop owing to reduction in effective cross-sectional area when they are contained in vertical specimens [20]. Moreover, anisotropic mechanical behavior might also be due to different preferential orientation of grains, but in the present investigation no strong crystallographic texture was observed in the examined samples by EBSD [24]. According to hardness results, a drop in strength is shown by solution annealed samples. As expected, isothermal aging leads to an intense increase in strength over the as built condition. The yield strength improved from 915 MPa of the as built steel to 1957 and 1793 MPa for samples peak-aged at 460 and 490 °C, respectively. On the contrary, fracture elongation underwent a drop from 6.1 % to 1.5 % and 1.2 % for the same materials.

Reversion of austenite during aging has been exploited in wrought maraging steels to increase ductility and fracture toughness [8]. In the SLMed samples of the present investigation, no strong enhancement in ductility was achieved even for prolonged aging time and high aging temperatures. It can be reasonably supposed that tiny size and fine dispersion of austenite found in SLM samples, as opposed to the micrometric pocket-like phases found in wrought alloys [6], is such to avoid a substantial toughening action as crack arrester phase, at least for the volume fractions here considered.

When evaluating the potential changes in toughness, it is also to consider that a further source of premature failure of the specimen can be related to the occasional presence of a certain amount of residual porosity (Figure 14), whereas in wrought alloys no porosity is expected. Porosity in SLM processed materials is mostly originated from pre-existing defects, mainly splats (large particles blown away from the molten pool and welded on adjacent zones of the built layer), which do not allow proper melting of the adjacent powder particles and prevent the homogeneous deposition of the following layers of the loose powder particles. It is expected that these un-melted zones might play a major role in reducing the ductility of metals, especially when low damage-tolerant materials are considered.

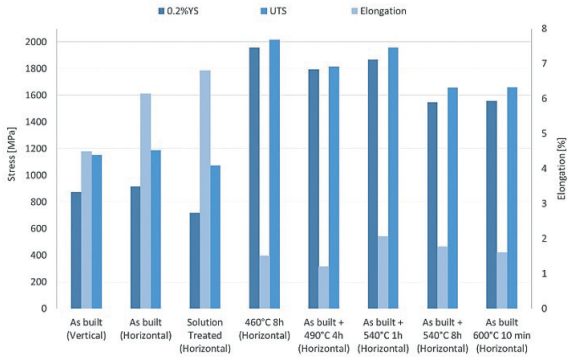

Fig. 13 - Tensile test results performed on as built solution annealed and aged samples.

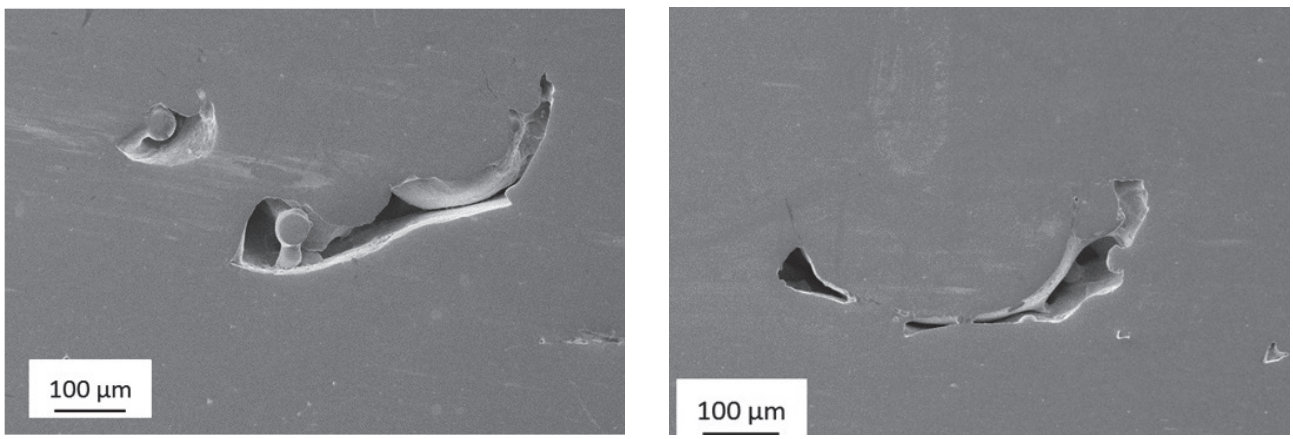

a. b.

Fig. 14 - Examples of pores found in the SLM produced vertically sectioned samples.

Analysis of the fracture surfaces of broken tensile specimens clearly show common features of ductile failure (Figure 15a and Figure 15b). Large voids and cavities mainly originated from the fusion defects above described, such as un-melted zones and splats (Figure 15c). In peak aged samples the development of cracks was mainly ruled by a cleavage decohesion mechanism, presumably across the martensite blocks (Figure 16).

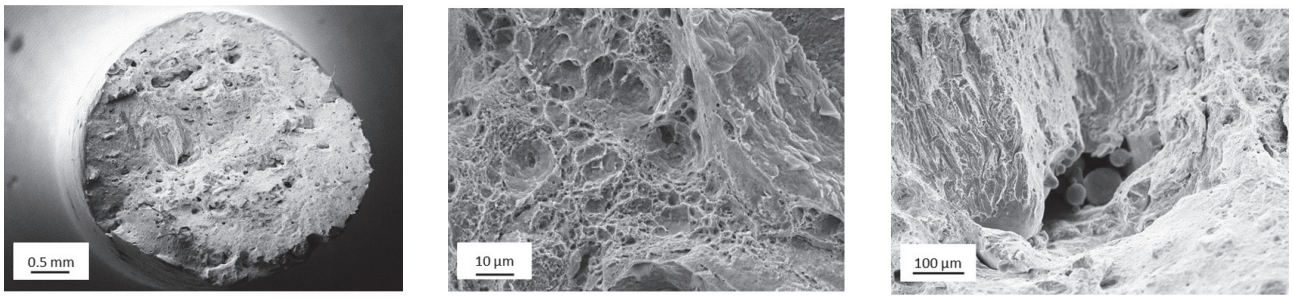

a. b. c.

Fig. 15 - Fracture surfaces of broken as build tensile specimen at (a) low and (b) high magnification. In picture (c) a magnification of a cavity containing un-melted powder particles is shown.

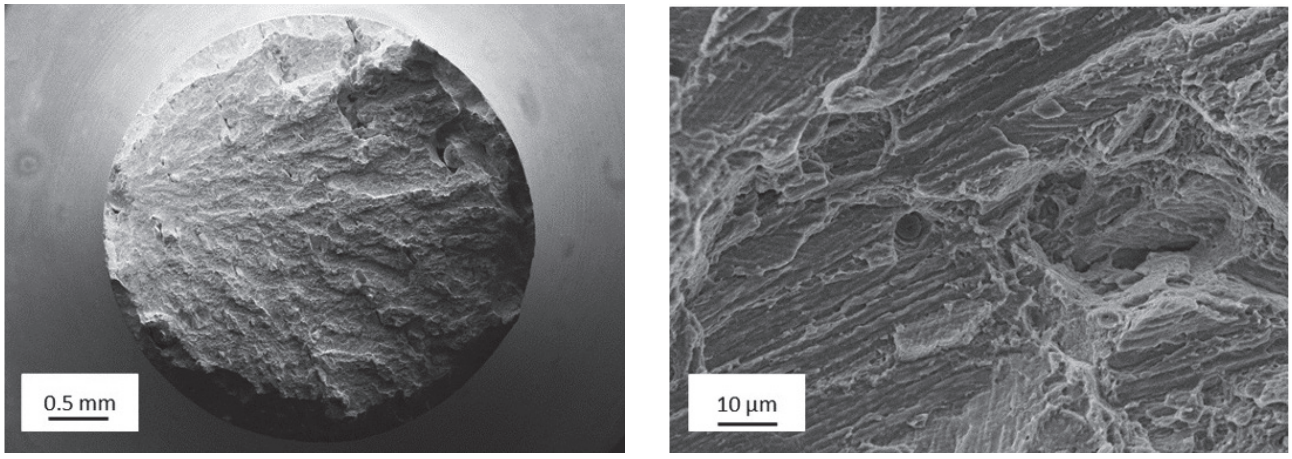

a. b.

Fig. 16 - Fracture surfaces of broken aged (460 °C, 8 h) tensile specimen at (a) low and (b) high magnification.

CONCLUSIONS

In this paper the microstructure, aging behavior, mechanical properties and fracture process of a SLM processed 18-Ni (300 grade) maraging steel were investigated. From results obtained, the following conclusions can be drawn.

i) A very fine cellular microstructure was detected in the as-built samples which was replaced by lath martensite structures organized into blocks after solution annealing.

ii) A comparison about the aging behaviour of the as-built and the solution-treated alloy revealed that the precipitation sequence during aging and hardness evolution are substantially equivalent even though small differences in activation energies for precipitate formation were observed.

iii) X-ray diffraction and microstructural analysis showed that aging promotes the partial reversion of martensite into austenite. Both temperature and time play a substantial role in increasing the austenite fraction.

iv) Aging promotes a drastic increase in strength over the as built condition along with a drop in tensile ductility. Changes in tensile strength and ductility are mainly governed by the effects given by the strengthening precipitates and microstructural defects, whereas the austenite reversion seems to be less effective.

v) The ductility and fracture behavior of the tensile specimen is strongly affected by the defect preferential orientation, as related to processing conditions. Splats and large droplets of remelted materials are occasionally deposited on the layer surface and promote interlayer defects such as porosity and cavities that particularly deplete the tensile ductility of specimens having their axis along the vertical direction.

ACKNOWLEDGEMENTS

The present research has been carried out with the contribution of Regione Lombardia through the project AddMe.Lab (call "Creatività, eventi e luoghi per l'innovazione nella moda e nel design, linea 2: infrastrutturazione fisica e digitale).

REFERENCES

1] J.M Pardal, S.S.M. Tavares, V.F. Terra, M.R. da Silva. D.R. dos Santos "Modeling of precipitation hardening during the aging and overaging of 18Ni-Co-Mo-Ti maraging 300 steel" J. Alloy. Compd. 393 (2015) 109–113.

2] W. Sha, A. Cerezo, G.D.W. Smith, "Phase Chemistry and Precipitation Reactions in Maraging Steels: Part I. Introduction and Study of Co-Containing C-300 Steel" Metall. Trans. A 24A (1993) 1221–1232.

3] J.M Pardal, S.S.M. Tavares, M.P.C. Fonseca, H.F.G. Abreu, J.J.J. Silva "Study of the austenite quantification by X-ray diffraction in the 18Ni-Co-Mo-Ti maraging 300 steel" J. Mater. Sci. 41 (2006) 2301–2307.

4] R. Tewari, S. Mazumder, I.S. Batra, G.K. Dey, S. Banerjee "Precipitation in 18 wt. % maraging steel of grade 350" Acta Mater. 48 (2000) 1187–1200.

5] X. Li, Z. Yin "Reverted austenite during aging in 18Ni (350) maraging steel" Mater. Lett. 24 (1995) 239–242.

6] U.K. Viswanathan, G.K. Dey, V. Sethumadhavan "Effects of austenite reversion during overageing on the mechanical properties of 18 Ni (350) maraging steel" Mater. Sci. Eng. A 398 (2005) 367–372.

7] D.D. Gu, W. Meiners, K. Wissenbach, R. Poprawe "Laser additive manufacturing of metallic components: materials, processes and mechanisms" Int. Mater. Rev. 57 (2012) 133–164.

8] Wohlers Report 2014 "3D Printing and Additive Manufacturing State of the Industry Annual Worldwide Progress Report" ISBN 978-0-9913332-0-2.

9] S.H. Huang, P. Liu, A. Mokasdar, L. Hou "Additive manufacturing and its societal impact: a literature review" Int. J. Adv. Manuf. Technol. 67 (2013) 1191–1203.

10] W.E. Frazier "Metal Additive Manufacturing: A Review" J. Mater. Eng. Perform. 23 (2014) 1917–1928.

11] P. Bassani, C. A. Biffi, R. Casati, A. Zanatta Alarcon, A. Tuissi, M. Vedani "Properties of Aluminium Alloys Produced by Selective Laser Melting" Key Engineering Materials 710 (2016) 83-88.

12] J.-P. Kruth, M. Badrossamay, E. Yasa, J. Deckers, L. Thijs, J. Van Humbeeck "Part and Material Properties in Selective Laser Melting of Metals", 16th International Symposium on Electromachining, Shanghai Jiao Tong University Press, 2010, Shanghai, China.

13] S. Das "Physical Aspects of Process Control in Selective Laser Sintering of Metals" Adv. Eng. Mater. 5 (2003) 701–711.

14] S.A. Khairallah, A.T. Anderson, A. Rubenchik, W.E. King "Laser powder-bed fusion additive manufacturing: Physics of complex melt flow and formation mechanisms of pores, spatter, and denudation zones" Acta Mater. 108 (2016) 36–45.

15] M.J. Starink "Analysis of aluminum based alloys by colorimetry: quantitative analysis of reactions and reaction kinetics" International Materials Reviews 49 (2004) 191-226.

16] L. Lutterotti "Total pattern fitting for the combined size-strain-stress-texture determination in thin film diffraction" Nuclear Inst. and Methods in Physics Research, B, 268, 334-340, 2010.

17] R. Casati, J. Lemke, A. Zanatta, M. Vedani "Aging Behavior of High-Strength Al Alloy 2618 Produced by Selective Laser Melting" Metallurgical and materials transaction A, doi:10.1007/s11661-016-3883-y.

18] E. Liverani, A. Fortunato, A. Leardini, C. Belvedere, S. Siegler, L. Ceschini, A. Ascari "Fabrication of Co–Cr–Mo endoprosthetic ankle devices by means of Selective Laser Melting (SLM)" Materials & Design 106 (2016) 60–68.

19] H. Schwab, F. Palm, U. Kühn, J. Eckert "Microstructure and mechanical properties of the near-beta titanium alloy Ti-5553 processed by selective laser melting" Materials & Design 105 (2016) 75–80.

20] R. Casati, J. Lemke, M. Vedani "Microstructure and Fracture Behavior of 316L Austenitic Stainless Steel Produced by Selective Laser Melting" Journal of Materials Science & Technology 32 (2016) 738–744.

21] D.D. Gu, Y.C. Hagedorn, W. Meiners, G. Meng, R.J. Santos Batista, K.Wissenbach, R. Poprawe "Densification behavior, microstructure evolution, and wear performance of selective laser melting processed commercially pure titanium" Acta Mater. 60 (2012) 3849–3860.

22] F. Verhaeghe, T. Craeghs, J. Heulens, L. Pandelaers "A pragmatic model for selective laser melting with evaporation" Acta Mater. 57 (2009) 6006–6012.

23] E. A. Jägle, Pyuck-Pa Choi, J. Van Humbeeck, D. Raabe "Precipitation and austenite reversion behavior of a maraging steel produced by selective laser melting" Journal of Materials Research 29 (2014) 2072-2079

24] R. Casati, J.N. Lemke, A. Tuissi, M. Vedani "Aging Behaviour and Mechanical Performance of 18-Ni 300 Steel Processed by Selective Laser Melting" Metals 6 (2016) 218

25] Guo Z, Sha W, Li D "Quantification of phase transformation kinetics of 18 wt.% ni C250 maraging steel" Materials Science & Engineering A, Structural Materials: Properties, Microstructure and Processing 373 (2004) 10-20.

26] Kapoor R, Batra IS "On the α' to γ transformation in maraging (grade 350) PH 13-8 and 17-4 PH steels" Materials Science & Engineering.A, Structural Materials: Properties, Microstructure and Processing 371 (2004) 324-34.

27] C. Menapace, I. Lonardelli, A. Molinari "Phase transformation in a nanostructured M300 maraging steel obtained by SPS of mechanically alloyed powders" Journal of Thermal Analysis and Calorimetry 101 (2010) 815-21.

28] C.R. Shamantha, R. Narayanan, K.J.L. Iyer, V.M. Radhakrishnan, S.K. Seshadri, S. Sundararajan, S. Sundaresan "Microstructural changes during welding and subsequent heat treatment of 18Ni (250-grade) maraging steel" Mater. Sci. Eng. A287 (2000) 43–51.